IOP Publishing Journal of Physics A: Mathematical and Theoretical
J. Phys. A: Math. Theor. **56** (2023) 165002 (28pp) https://doi.org/10.1088/1751-8121/acc3cf

Survival in a nanoforest of absorbing pillars

Denis S Grebenkov[1,*] **and Alexei T Skvortsov**[2]

[1] Laboratoire de Physique de la Matière Condensée, CNRS, Ecole Polytechnique, Institut Polytechnique de Paris, 91120 Palaiseau, France
[2] Maritime Division, Defence Science and Technology Group, 506 Lorimer Street, Fishermans Bend, Victoria 3207, Australia

E-mail: denis.grebenkov@polytechnique.edu

Received 3 January 2023; revised 23 February 2023
Accepted for publication 13 March 2023
Published 24 March 2023

Abstract

We investigate the survival probability of a particle diffusing between two parallel reflecting planes toward a periodic array of absorbing pillars. We approximate the periodic cell of this system by a cylindrical tube containing a single pillar. Using a mode matching method, we obtain an exact solution of the modified Helmholtz equation in this domain that determines the Laplace transform of the survival probability and the associated distribution of first-passage times (FPTs). This solution reveals the respective roles of several geometric parameters: the height and radius of the pillar, the inter-pillar distance, and the distance between confining planes. This model allows us to explore different asymptotic regimes in the probability density of the FPT. In the practically relevant case of a large distance between confining planes, we argue that the mean FPT is much larger than the typical time and thus uninformative. We also illustrate the failure of the capacitance approximation for the principal eigenvalue of the Laplace operator. Some practical implications and future perspectives are discussed.

Keywords: diffusion-controlled reactions, first-passage time, spiky coating, pillar, nanoforest, survival probability, modified Helmholtz equation

(Some figures may appear in colour only in the online journal)

1. Introduction

When a particle diffuses through a complex environment filled with traps, its survival probability, which determines the first-passage time (FPT) distribution, depends on the geometric configuration in a very sophisticated way [1–13]. Most former theoretical studies were focused

* Author to whom any correspondence should be addressed.

on the mean FPT or, equivalently, on the overall reaction rate on that traps (see [14–20] and references therein). Despite the impressive progress in understanding the mean FPT for various stochastic processes, its dominant role as a unique timescale determining the whole distribution has been questioned [21–24]. In fact, even though the mean FPT characterizes well the diffusive exploration of a bounded confining domain, the absorption or reaction event may occur on much shorter time scales. For instance, in the physiologically relevant example of calcium diffusion towards calcium-sensing receptors inside a presynaptic bouton, the mean FPT is usually around tens of milliseconds, whereas the typical FPT is two or even three orders of magnitude shorter [25]. The limited role of the mean FPT is particularly clear for unbounded domains, for which the mean FPT is infinite due to a large contribution of rare long trajectories. The whole distribution of the FPT is therefore required for a systematic comprehension of diffusion-controlled reactions and related search processes.

For this purpose, many efforts were dedicated to characterize the long-time behavior of the survival probability in disordered or random environments [3, 26, 27] such as random packs of absorbing immobile spheres [28–30], near a fractal boundary [31], or in dynamic heterogeneous media [32]. The random trajectories that survived up to long times thoroughly explore the confining environment and thus keep some averaged information on its geometric structure. Their contribution to the survival probability determines the right tail of the probability density function (PDF) of the FPT. In turn, the short-time behavior of the survival probability is controlled by so-called 'direct trajectories' which are close to the shortest geodesic path between the starting point and the closest trap [22, 33, 34]. Such trajectories are therefore sensitive only to the local geometric structure, yielding rather universal short-time behavior in the left tail of the PDF. Its mathematical description goes back to the seminal works by Varadhan [35, 36] and resembles the concepts of geometric optics in physics [37, 38].

In contrast, the whole distribution of the FPT, that encompasses all time- and geometric length scales, is known exactly only for rather simple configurations such as an interval, a rectangle, a disk, a sphere, or a pair of coaxial cylinders or concentric spheres [1, 39–41]. In these settings, the symmetry of the confining domain allows for a separation of variables and leads to explicit representations of the survival probability and the PDF of the FPT. When the absorbing region is only a part of the otherwise reflecting boundary, such basic methods do not work anymore, and one has to employ more sophisticated tools. For instance, Isaacson and Newby proposed a uniform in time asymptotic expansion for the PDF of the FPT to a small target [42]. Another approach was used in [43] to compute the survival probability inside two-dimensional rotationally invariant domains (like a disk or a sector) in the presence of an absorbing arc on the boundary. Both an exact solution relying on a matrix inversion, and an approximate explicit solution were proposed. In the case of domains formed by coaxial cylinders or concentric spheres, the survival probability in the presence of an absorbing region was obtained with the aid of the self-consistent approximation [44–46]. A general method for getting the survival probability in a medium with multiple spherical traps was described in [47].

In a recent paper [48], we studied steady-state diffusion from a remote source towards a periodic array of absorbing identical cylindrical pillars protruding from a flat base (figure 1(a)). Using a mode matching method [49–51], we solved the underlying Laplace equation and found the exact form of the diffusive flux onto each pillar, $J = c_0 D\mathcal{A}/(L_2 + z_0)$, where c_0 is the imposed concentration of particles at the source, D is the diffusion coefficient, $\mathcal{A}$ is the cross-sectional area of a periodic cell, L_2 is the distance between the source and the top of the pillars, and z_0 is the offset parameter that aggregates the geometric complexity and reactivity of the spiky coating. Using the exact though sophisticated expression for z_0, we analyzed the behavior of the steady-state diffusive flux in different asymptotic regimes.

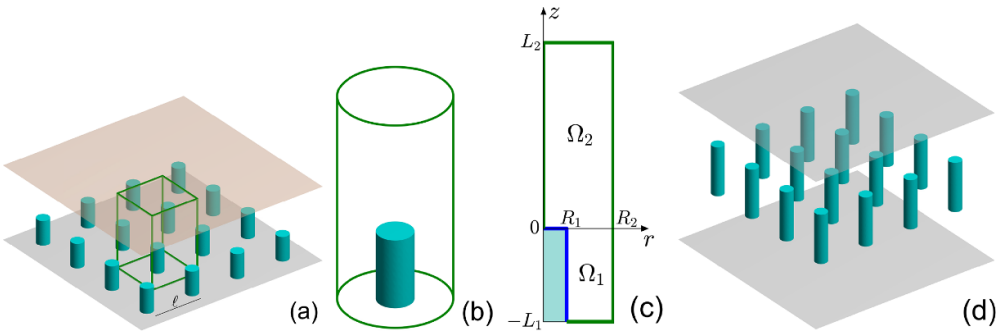

Figure 1. (a) A square-lattice array of cylindrical pillars (in light blue) on a reflecting support (in gray), capped by an upper reflecting plane (in pink). Periodicity of this domain allows one to focus on diffusion in a periodic cell around one pillar—a green rectangular parallelepiped. (b) A single pillar surrounded by an effective coaxial reflecting cylindrical tube and capped by two parallel reflecting planes. (c) Planar (xz) projection of the three-dimensional domain from panel (b). Blue segments show the absorbing pillar and green segments represent reflecting parts (the green vertical segment at $r = 0$ is also reflecting to respect the regularity and the axial symmetry of the solution, see appendix A.1). Shadowed (light blue) region is the solid (inaccessible) interior of the cylindrical pillar. Here R_2 is the radius of the outer reflecting cylinder, R_1 is the radius of the absorbing pillar, L_1 is its height, and L_2 is the distance between the source and the top of the pillar (i.e. $L_1 + L_2$ is the height of the whole system). Note that R_2 is related to the inter-pillar distance ℓ, e.g. $R_2 = \ell/\sqrt{\pi}$ for the square lattice. (d) An equivalent problem of twice longer pillars between two reflecting planes separated by distance $2(L_1 + L_2)$.

In the present work, we extend the above analysis to the modified Helmholtz equation, $(p - D\Delta)u = 0$, which describes diffusion in a reactive medium with the bulk reaction rate p; in addition, this equation results from the Laplace transform of the diffusion equation $\partial_t c = D\Delta c$ and thus gives access to time-dependent diffusion. In particular, we focus on the survival probability of a particle diffusing towards a nanoforest of absorbing pillars. We obtain the exact solution for the Laplace transform of this quantity that yields the moments and the PDF of the FPT to absorbing pillars.

The paper is organized as follows. In section 2, we formulate the problem and describe the main steps of its solution. Section 3 presents several properties of the FPT distribution. In particular, we discuss the short-time and long-time asymptotic behaviors of the PDF of the FPT, the limited significance of the mean FPT, the failure of the capacitance approximation for the decay time, and the respective roles of different geometric parameters of the nanoforest. Conclusions and open problems are summarized in section 4. Details of the derivation are re-delegated to appendices.

2. Exact solution

We consider ordinary diffusion of a point-like particle between two reflecting planes at $z = -L_1$ and $z = L_2$ in three dimensions. The bottom plane is covered by a square-lattice array of absorbing identical cylindrical pillars of radius R_1 and height L_1, with the inter-pillar distance ℓ between the centers of the closest pillars (figure 1(a)). The periodicity of this array allows one to focus on diffusion in a periodic cell containing a single pillar, i.e. inside a rectangular parallelepiped $(-\ell/2, \ell/2)^2 \times (-L_1, L_2)$ with periodic boundary conditions along x and y directions. Following the rationale by Keller and Stein [52], we replace this original

periodic cell by a cylindrical tube with reflecting boundary condition. The radius R_2 of the tube is chosen to preserve the volume of the periodic cell by setting $\pi R_2^2 = \ell^2$. In this way, we will approximate the solution of the original problem by the exact solution of the reduced problem. The accuracy of this approximation can be accessed by a numerical solution of the original problem. Its systematic study will be presented elsewhere (see the related discussion in [53] for the Laplace equation in a different geometric setting).

From now on, we focus on diffusion inside a bounded domain Ω, surrounded by a cylindrical tube of radius R_2, towards a co-axial cylindrical absorbing pillar of radius R_1 and height L_1, both confined between parallel reflecting planes at $z = -L_1$ and $z = L_2$ (figure 1(b)). Starting from a point $\boldsymbol{x}$ inside this confining domain, the particle moves with the diffusion coefficient D until the first arrival onto the surface of the pillar. The FPT to that surface, τ, is a random variable, which is fully characterized by the survival probability, $S(t|\boldsymbol{x}) = \mathbb{P}\{\tau > t\}$. The latter satisfies the (backward) diffusion equation, $\partial_t S = D\Delta S$, which is supplemented by the initial condition $S(0|\boldsymbol{x}) = 1$ and mixed boundary conditions: $S(t|\boldsymbol{x}) = 0$ on the absorbing pillar, and $\partial_z S(t|\boldsymbol{x}) = 0$ on the reflecting planes. The negative time derivative, $H(t|\boldsymbol{x}) = -\partial_t S(t|\boldsymbol{x})$, is the PDF of the FPT τ. In turn, the Laplace transform of the survival probability,

$$\tilde{S}(p|\boldsymbol{x}) = \int_0^\infty \mathrm{d}t\, e^{-pt} S(t|\boldsymbol{x}), \tag{1}$$

satisfies the modified Helmholtz equation, subject to the same boundary conditions. More explicitly, we search for the Laplace-transformed survival probability that satisfies the following boundary value problem in cylindrical coordinates $\boldsymbol{x} = (r, z, \phi)$:

$$(p - D\Delta)\tilde{S} = 1 \quad \text{in } \Omega, \tag{2a}$$

$$\tilde{S} = 0 \quad (r < R_1,\ z = 0), \tag{2b}$$

$$\tilde{S} = 0 \quad (r = R_1,\ -L_1 < z < 0), \tag{2c}$$

$$\partial_z \tilde{S} = 0 \quad (0 < r < R_2,\ z = L_2), \tag{2d}$$

$$\partial_z \tilde{S} = 0 \quad (R_1 < r < R_2,\ z = -L_1), \tag{2e}$$

$$\partial_r \tilde{S} = 0 \quad (r = R_2,\ -L_1 < z < L_2), \tag{2f}$$

where $\Delta = \partial_r^2 + (1/r)\partial_r + \partial_z^2$ is the Laplace operator in cylindrical coordinates (without the angular part). Here, equations (2*b*) and (2*c*) incorporate absorption on the pillar, while equations (2*d*)–(2*f*) describe reflections of the particle on the top and bottom boundaries and on the outer cylindrical surface. The rotation invariance of this problem implies that $\tilde{S}(p|r,z)$ does not depend on the angle ϕ, which therefore will be omitted in what follows. Note also that the reflection with respect to the plane at $z = -L_1$ transforms this geometric setting into an equivalent one, with a twice longer pillar located in the middle of the cylindrical tube of height $2(L_1 + L_2)$. In other words, we also approximate the Laplace-transformed survival probability in the presence of twice longer absorbing pillars located in the middle between two parallel reflecting planes (figure 1(d)).

Setting $\tilde{S}(p|r,z) = (1 - \tilde{H}(p|r,z))/p$, one can transform the above inhomogeneous modified Helmholtz equation into the homogeneous one:

$$(p - D\Delta)\tilde{H} = 0 \quad \text{in } \Omega, \tag{3a}$$

$$\tilde{H} = 1 \quad (r < R_1,\ z = 0), \tag{3b}$$

$$\tilde{H} = 1 \quad (r = R_1,\ -L_1 < z < 0), \tag{3c}$$

$$\partial_z \tilde{H} = 0 \quad (0 < r < R_2,\ z = L_2), \tag{3d}$$

$$\partial_z \tilde{H} = 0 \quad (R_1 < r < R_2,\ z = -L_1), \tag{3e}$$

$$\partial_r \tilde{H} = 0 \quad (r = R_2,\ -L_1 < z < L_2). \tag{3f}$$

In this way, we focus directly on the Laplace transform $\tilde{H}(p|r,z)$ of the PDF $H(t|r,z)$ of the FPT. Since $\tilde{H}(p|r,z) = \mathbb{E}\{e^{-p\tau}\}$, the derivatives of this function with respect to p determine the integer-order moments of the FPT:

$$\mathbb{E}\{\tau^k\} = (-1)^k \lim_{p\to 0} \frac{\partial^k \tilde{H}(p|r,z)}{\partial p^k}. \tag{4}$$

Moreover, the function $\tilde{H}(p|r,z)$ admits another interpretation as a steady-state concentration of particles, emitted from the pillar into a reactive medium with the bulk reactivity p. Yet another probabilistic interpretation is that $\tilde{H}(p|r,z)$ is the probability for a particle started from $\boldsymbol{x} = (r,z,\phi)$ to arrive onto the pillar before being killed in the bulk. In other words, it describes the survival of a mortal random walker [54–57].

In appendix A, we derive the exact solution of the problem (3) by using a mode matching method [48–51]. In a nutshell, one represents a general solution of equation (3*a*) in subdomains with $z < 0$ and $z > 0$ as two series (A.2) and (A.11) involving appropriate Bessel functions. The continuity and differentiability of the solution at the junction $z = 0$ imply an infinite system (A.29) of linear algebraic equations on the unknown coefficients of these series. The elements of the infinite-dimensional matrix W that defines this system, are known explicitly through equation (A.30). Truncating this system to a finite size N, one can solve it numerically by inverting a finite-size matrix. Despite the need for a numerical step, the obtained solution provides an analytic dependence of $\tilde{H}(p|r,z)$ on the coordinates r and z of the starting point. Moreover, the truncation error rapidly decreases with N, allowing one to use moderate truncation orders (say, few tens) and thus very rapid computations for a broad range of parameters. Finally, the structure of the solution reveals the respective roles of different parameters and opens a way to asymptotic analysis. In the following, we mainly focus on the PDF $H(t|r,z)$ that can be obtained numerically by representing the inverse Laplace transform of $\tilde{H}(p|r,z)$ as the Bromwich integral and approximating it with the help of the Talbot algorithm [58]. We fixed the truncation size $N = 10$ and checked that this choice was sufficient to get accurate results.

As diffusion occurs in a bounded domain, the survival probability and the PDF of the FPT admit general spectral expansions:

$$S(t|r,z) = \sum_{n=0}^{\infty} e^{-Dt\lambda_n} u_n(r,z) \int_\Omega \mathrm{d}\boldsymbol{x}\, u_n(\boldsymbol{x}) \tag{5}$$

and

$$H(t|r,z) = \sum_{n=0}^{\infty} D\lambda_n\, e^{-Dt\lambda_n} u_n(r,z) \int_\Omega \mathrm{d}\boldsymbol{x}\, u_n(\boldsymbol{x}), \tag{6}$$

where λ_n and $u_n(\boldsymbol{x})$ are the eigenvalues and $L_2(\Omega)$-normalized eigenfunctions of the (negative) Laplace operator $-\Delta$. The eigenvalues, which are positive and enumerated in an ascending order, are determined by the poles $\{p_n\}$ of $\tilde{S}(p|r,z)$ as $\lambda_n = -p_n/D$. In turn, the poles are obtained as the values of p in the complex plane $\mathbb{C}$, at which the matrix $I + W$ is not invertible, i.e. when $\det(I + W) = 0$ (with I being the identity matrix). As the eigenvalues are positive,

one can search for the poles p_n on the negative axis (see details in appendix A.4). In turn, the eigenfunctions and the coefficients (given by the integral) are determined from the residues of $\tilde{S}(p|r,z)$ at the poles. Despite the simple intuitively appealing form of these spectral expansions, their numerical computation is tedious so that we performed a numerical inversion of the Laplace transforms $\tilde{S}(p|r,z)$ and $\tilde{H}(p|r,z)$, as described above.

3. Discussion

In this section, we discuss the properties of the survival probability $S(t|r,z)$ and the PDF $H(t|r,z)$ of the FPT. In particular, we aim at understanding the respective roles of different geometric parameters of the system, namely, the pillar's radius R_1 and height L_1, the distance L_2 to the top reflecting plane, and the radius R_2 of the outer reflecting surface, which is related to the inter-pillar distance ℓ. Throughout this discussion, we fix the radius R_2 and rescale all other lengths by R_2. While the obtained exact solution is valid for any set of these parameters, we will mainly focus on configurations, in which L_2/R_2 is large and $\rho = R_1/R_2$ is small. In all numerical examples, we set $R_2 = 1$ and $D = 1$ to fix units of length and time.

We generally discuss the whole distribution of the FPT and its asymptotic behaviors. As said earlier, the short-time asymptotic behavior is determined by 'direct trajectories' that go straight from the starting point to the closest point on the pillar [22, 23]. As a consequence, the left tail of the PDF is very sensitive to the starting point and to the closest part of the pillar. In turn, the geometric configuration of the system does not almost affect this behavior. As earlier discussed for other settings [24, 44–46], one generally gets the Lévy–Smirnov type behavior,

$$H(t|r,z) \sim \frac{\delta}{\sqrt{4\pi D t^3}} e^{-\delta^2/(4Dt)} \qquad (t \to 0), \tag{7}$$

where δ is the distance between the starting point and the absorbing pillar. As this short-time behavior is rather universal, we do not dwell on its analysis. In contrast, we focus on the intermediate- and long-time behaviors when the particle has enough time to explore the bulk around the pillar and is thus sensitive to the geometric configuration of the system.

3.1. Long-time behavior

The spectral expansion (6) implies an exponential decay of the PDF at long times:

$$H(t|r,z) \approx \frac{e^{-t/T}}{T} u_0(r,z) \int\limits_{\Omega} \mathrm{d}\boldsymbol{x}\, u_0(\boldsymbol{x}), \tag{8}$$

where the decay time $T = 1/(D\lambda_0)$ is determined by the principal (smallest) eigenvalue λ_0, which depends on the geometric parameters of the domain Ω is a sophisticated way.

To get some insights onto the decay time, let us first establish a simple upper bound. If the starting point $\boldsymbol{x}$ is located in the upper part of the domain (with $z > 0$), the survival probability obeys the following inequality:

$$S(t|r,z) \geqslant S_1(t|z) \qquad (t \geqslant 0,\ z > 0), \tag{9}$$

where $S_1(t|z)$ is the survival probability in a capped cylinder of radius R_2 with an absorbing disk at $z = 0$ and a reflecting disk at $z = L_2$. Due to the axial symmetry, this is actually the survival probability on the interval $(0, L_2)$ with the absorbing endpoint 0 and the reflecting endpoint L_2. This inequality follows from the continuity of Brownian motion: any trajectory that hits the absorbing pillar at time t should cross the level $z = 0$ and thus hit the disk at an earlier

time t', i.e. it is more probable to avoid the contact with the pillar than the contact with the absorbing disk at $z=0$. The survival probability $S_1(t|z)$ is known explicitly (see, e.g. [1]) and is reproduced in equation (B.1) for completeness. In particular, it decays exponentially at long times, with the decay rate $D\pi^2/(4L_2^2)$. To ensure the inequality (9), the decay rate of $S(t|r,z)$ should be slower than (or equal to) the decay rate of $S_1(t|z)$, i.e. $\lambda_0 \leqslant \pi^2/(4L_2^2)$. Similarly, if the particle starts from a point with $r > R_1$, the survival probability obeys another inequality:

$$S(t|r,z) \geqslant S_2(t|r) \qquad (t \geqslant 0,\ r > R_1), \tag{10}$$

where $S_2(t|r)$ is the survival probability inside the annulus between an absorbing circle of radius R_1 and a reflecting circle of radius R_2. Once again, before hitting the pillar, any trajectory started from a point with $r > R_1$ must cross the cylindrical surface at $r = R_1$, whatever the vertical coordinate is. The survival probability $S_2(t|r)$ in the annulus also admits an explicit solution (see, e.g. [41]) and is reproduced in equation (B.2). Its long-time behavior is determined by the decay rate $D\alpha_{0,1}^2/R_2^2$ so that $\lambda_0 \leqslant \alpha_{0,1}^2/R_2^2$, where $\alpha_{0,1}$ is the smallest positive solution of equation (A.9). Combining two inequalities, we get the following lower bound for the decay time:

$$T \geqslant \max\left\{\frac{R_2^2}{\alpha_{0,1}^2 D}, \frac{4L_2^2}{\pi^2 D}\right\}. \tag{11}$$

Depending on the geometric parameters, either of two bounds can be dominant. If the pillar is very thin, $\alpha_{0,1}^2$ is small, so that $R_2^2/(\alpha_{0,1}^2 D)$ can be the maximum, if L_2/R_2 is not too large (see further discussion in section 3.5). In contrast, if L_2/R_2 is large enough, $4L_2^2/(\pi^2 D)$ is the maximum. Since $\alpha_{0,1}^2$ decreases logarithmically slowly as $R_1 \to 0$ according to equation (19), the latter case is more relevant for applications. Note also that the upper bound does not depend on the pillar's height L_1; one can therefore expect that the impact of this geometric parameter onto the decay time is moderate, at least in the settings with large L_2/R_2. We return to this point in section 3.3.

3.1.1. Mean FPT. When the target is small (as compared to the confining domain), the decay time T is usually close to the mean FPT. In the regime $L_2/R_2 \gg 1$, there is a simple approximation for the mean FPT. In fact, a spiky bottom surface can be approximated by an effective absorbing flat boundary located at $z = -z_0$, where the offset parameter z_0 was thoroughly investigated in [48]. In this way, the original problem is reduced to one-dimensional diffusion on the interval $(-z_0, L_2)$ with the absorbing endpoint $-z_0$ and the reflecting endpoint L_2, for which the mean FPT is:

$$T(z) = \frac{(z+z_0)(2L_2 + z_0 - z)}{2D}. \tag{12}$$

Moreover, if the starting point is uniformly distributed, the volume average of $T(z)$ yields $\overline{T} = (L_2 + z_0)^2/(3D)$, where z_0 incorporates the dependence on the geometric parameters of the system. As z_0 is usually much smaller than L_2, one has $\overline{T} \approx \frac{1}{3}L_2^2/D$, which is close to the lower bound $\frac{4}{\pi^2}L_2^2/D$ on the decay time T.

3.1.2. Capacitance approximation. When the pillar is small as compared to the cylindrical tube, i.e. $L_1/R_2 \ll 1$ and $\rho = R_1/R_2 \ll 1$, the reflecting boundary can be treated as being at infinity, and one often approximates the principal eigenvalue as [59–63]:

$$\lambda_0 \approx \frac{\mathcal{C}}{|\Omega'|}, \tag{13}$$

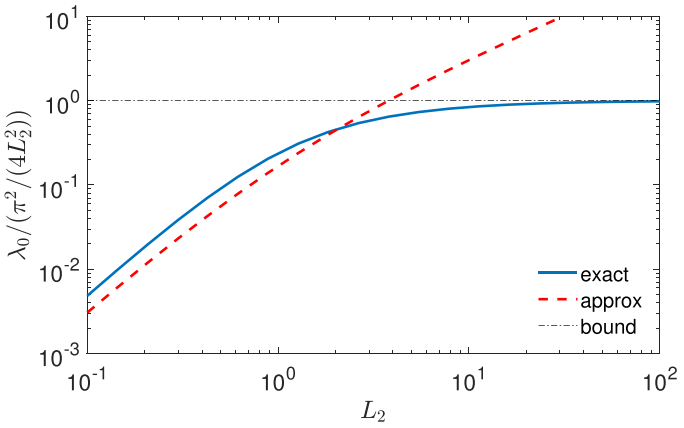

Figure 2. Principal eigenvalue λ_0 of the Laplace operator, rescaled by its upper bound $\pi^2/(4L_2^2)$, as a function of L_2, for the domain with $R_1 = 0.1$, $L_1 = 1$ and $R_2 = 1$. The eigenvalue λ_0 (shown by solid line) was obtained as $-p_0/D$, where p_0 is the pole of $\tilde{S}(p|r,z)$ with the smallest absolute value, which was found numerically as the first zero of $\det(I+W) = 0$ (see appendix A.4). Dashed line presents the capacitance approximation (13), while dash–dotted horizontal line indicates the upper bound (here, it is located at 1 due to rescaling).

where $|\Omega'| = 2|\Omega| = 2\pi\,(L_1(R_2^2 - R_1^2) + L_2R_2^2)$ is the volume of the twice bigger domain Ω', which is obtained by reflection with respect to the plane at $z = -L_1$, and $\mathcal{C}$ is the capacitance of the twice longer pillar [64]:

$$\mathcal{C} = 4\pi R_1 \frac{1 + (L_1/R_1)^2}{\frac{\pi}{2} + \frac{L_1}{R_1}\ln\frac{L_1}{R_1}} \tag{14}$$

(note that we use the convention, in which the capacitance of a sphere of radius r is $4\pi r$). As a consequence, the capacitance approximation (13) implies the following expression for the decay time:

$$T_{\text{cap}} = \frac{L_2R_2}{2D}\,\frac{1 + (1-\rho^2)L_1/L_2}{\rho\left(\frac{1+(L_1/R_1)^2}{\pi/2+(L_1/R_1)\ln(L_1/R_1)}\right)}\,. \tag{15}$$

In the same vein, the capacitance was employed to describe the mean FPT, the overall reaction rate, and the long-time behavior of the survival probability (see [65–68] and references therein).

However, one can see that this approximation is incompatible with the lower bound (11) in the regime $L_2/R_2 \gg 1$. In fact, the decay time T_{cap} grows linearly with L_2 when other parameters are fixed, whereas the lower bound grows quadratically with L_2. This is a striking example of the failure of the capacitance approximation (13) for anisotropic confining domains. In other words, when speaking about the small target limit, one has to take the double limit $L_2 \to \infty$ and $R_2 \to \infty$ simultaneously to keep the confining domain more or less isotropic.

Figure 2 illustrates the behavior of the principal eigenvalue λ_0 as a function of L_2. It is rescaled by $\pi^2/(4L_2^2)$ to highlight the role of this upper bound. One sees that λ_0 rapidly approaches its upper bound as L_2 increases. In turn, the capacitance approximation (13) captures qualitatively the behavior of λ_0 when $L_2 \lesssim 2$ but then exceeds the upper bound and thus fails. Note that the shift between two curves at small L_2 is caused by the fact that the target is not small

enough as compared to the confining domain (here, $R_1/R_2 = 0.1$ and $L_1/R_2 = 1$). For smaller R_1/R_2 and/or L_1/R_2 (not shown), the agreement in the region of small L_2 is better, but the capacitance approximation still fails at large L_2.

3.1.3. Role of the decay time. We conclude that if L_2/R_2 is large, the decay time T is close to its lower bound $\frac{4}{\pi^2}L_2^2/D$. Most importantly, it does not almost depend on the geometric parameters of the system (except L_2), i.e. this time scale is uninformative for the considered first-passage process. Similarly, the mean FPT, which is usually close to the decay time, does not bear substantial information on the search process in this case. Moreover, in the limit $L_2 \to \infty$, the decay time and the mean FPT diverge and therefore become useless. For this reason, we do not discuss the mean FPT in the remaining text and focus on the whole distribution.

3.2. Role of distance L_2

In many applications, the distance L_2 is much larger than the other length scales. An interesting question is how the long-time behavior changes as L_2 goes to infinity. In this limit, the principal eigenvalue λ_0 vanishes so that the exponential decay (8) should transform into a slower decrease at $L_2 = \infty$. In the particular case $R_1 = R_2$, the original three-dimensional problem reduces to one-dimensional diffusion on the positive semi-axis $\mathbb{R}_+$, with the Lévy–Smirnov PDF:

$$H_{1D}(t|z) = \frac{ze^{-z^2/(4Dt)}}{\sqrt{4\pi Dt^3}}, \tag{16}$$

behaving as $t^{-3/2}$ as $t \to \infty$ [1]. The origin of this slow power-law decay is the existence of very long random trajectories that can go arbitrarily far away from the absorbing point at $z = 0$. Even though such long trajectories are unlikely, their contribution makes the mean FPT infinite. The same probabilistic argument holds in the case $R_1 < R_2$ so that the PDF $H(t|r,z)$ behaves as $t^{-3/2}$ in general. In appendix A.3, we deduce this general behavior from the exact solution. To grasp the origin of this slow power-law decay without technical analysis, one can again apply the inequality (9), in which $S_1(t|z)$ is now the survival probability on the positive semi-axis, which is known exactly:

$$S_{1D}(t|z) = \mathrm{erf}\left(\frac{z}{\sqrt{4Dt}}\right), \tag{17}$$

where $\mathrm{erf}(z)$ is the error function. At long times, one has $S_{1D}(t|z) \approx z/\sqrt{\pi Dt}$ so that the survival probability $S(t|r,z)$ cannot decrease faster than $t^{-1/2}$. This simple argument excludes, e.g. an exponential decay of $S(t|r,z)$ in the limit $L_2 = \infty$.

Figure 3(a) illustrates the effect of an increasing distance L_2 onto the probability density $H(t|r,z)$. The starting point is located above the top of the pillar, at a height $z = 1$. At short times, only 'direct' trajectories to the pillar contribute to the left tail of the PDF so that the distance L_2 to the top boundary does not matter, and all three curves coincide. In contrast, the long-time limit corresponds to a diffusive exploration of the bounded domain so that an increase of L_2 strongly affects the right tail, shifting it to longer times. Even though there is an exponential cut-off for any finite L_2, one can clearly see the emergence of an intermediate regime with a power-law decay $t^{-3/2}$, starting from $t \gtrsim 1$, in agreement with the above analysis. This behavior can be recognized by a straight line in the log-log plot; for comparison, equation (16) is also shown. One sees that the exponential cut-off is progressively shifted to the right as L_2 increases, thus confirming that the PDF in the limit $L_2 = \infty$ exhibits the same power-law decay at any long enough time t.

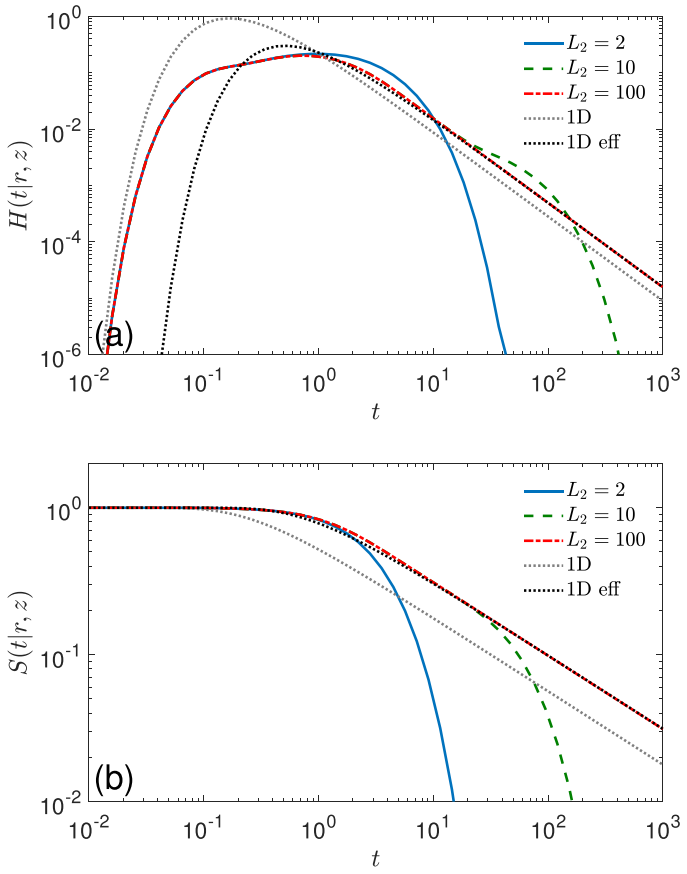

Figure 3. (a) Probability density $H(t|r,z)$ of the FPT to the absorbing pillar, with $R_1 = 0.1$, $L_1 = 10$, $r = 0$, $z = 1$, and three values of L_2 (see the legend). Gray and black dotted lines present respectively the probability densities $H_{1D}(t|r,z)$ and $H_{1D}(t|r,z+z_0)$ from equation (16) for the half-line, illustrating the emergence of a power-law shoulder before an exponential cut-off. The offset parameter $z_0 \approx 0.75$ was calculated by the exact formula given in [48]. (b) Survival probability $S(t|r,z)$ and its approximations $S_{1D}(t|z)$ and $S_{1D}(t|z+z_0)$ given by equation (17) for the same setting.

Curiously, the straight part of the curve corresponding to $H(t|r,z)$ lies above the PDF $H_{1D}(t|z)$ for the half-line; one can therefore conclude that the probability of hitting a thin pillar at time t (large enough) is actually bigger than that for a thick pillar (with $R_1 = R_2$). This result sounds counter-intuitive. To rationalize it, let us first recall again that the steady-state flux on a spiky surface is equal to the steady-state flux on an equivalent absorbing flat surface located at $z = -z_0$, where $z_0 \geqslant 0$ is the offset parameter [48]. As a consequence, the long-time behavior of the PDF $H(t|r,z)$ can be approximated by that of $H_{1D}(t|z+z_0)$ for the half-line with the origin at $-z_0$, not at 0. This is confirmed by the black dotted curve that shows $H_{1D}(t|z+z_0)$. Indeed, this curve lies above $H_{1D}(t|z)$ at long times thanks to the larger prefactor $z+z_0$. This behavior can be rationalized in probabilistic terms. In fact, any random trajectory that hits the absorbing point $-z_0$ at time t has to cross the intermediate level $z = 0$ at an earlier time t'. As the probability density $H_{1D}(t|z)$ monotonously decreases at

large t, one has $H_{1D}(t|z+z_0) = H_{1D}(t'|z) > H_{1D}(t|z)$. For comparison, figure 3(b) shows the corresponding survival probability $S(t|r,z)$ and its approximations $S_{1D}(t|z)$ and $S_{1D}(t|z+z_0)$, given by equation (17).

In the following, we assume that L_2 is large enough so that the right tail of the PDF can be approximated by $(z+z_0)/\sqrt{4\pi Dt^3}$ (with $z>0$) over a broad range of times. In this case, the mean FPT is very large (of the order of L_2^2/D) and is thus not informative.

3.3. Role of height L_1

In the previous subsection, we saw how an increase of L_2 transforms an exponential decay of the PDF into a power-law decay. This is a direct consequence of the fact that the confining domain Ω becomes unbounded in the limit $L_2 \to \infty$. Alternatively, the confining domain Ω can be made unbounded by taking the limit $L_1 \to \infty$ (with a large but fixed L_2). In this limit, however, the exponential decay persists even for $L_1 = \infty$. In fact, if one formally sets $L_2 \to 0$, the problem is reduced to diffusion in a semi-infinite tube containing a semi-infinite absorbing pillar. Due to the reflecting boundary at $z = L_2$, this is equivalent to diffusion in an infinite tube with an infinite pillar, for which diffusion along the tube axis z does not matter, and the survival probability is determined by diffusion in the cross-section, i.e. in an annulus between an inner absorbing circle and an outer reflecting circle. Despite the fact that the domain is unbounded, this survival probability admits a spectral expansion (B.2) and exhibits an exponential decay at long times. The decay rate is given by the principal eigenvalue $\lambda_0 = \alpha_{0,1}^2/R_2^2$, where $\alpha_{0,1}$ is the smallest zero of equation (A.9). This argument can be extended to any finite $L_2 > 0$, for which the particle has an additional space $0 < z < L_2$ for diffusion, so that it is easier to survive and thus $\lambda_0 \leqslant \alpha_{0,1}^2/R_2^2$, in agreement with the earlier established bound (11). At the end of appendix A.3, we provide additional analytic arguments why there is no power-law decay in the limit $L_1 \to \infty$ for any finite L_2.

Figure 4(a) shows the PDF $H(t|r,z)$ for three values of L_1. To eliminate the impact of the tube height, we set $L_2 = 100$ and keep the starting point to be above the pillar, with $r = 0$ and $z = 1$. One can see that the pillar's height L_1 has a low impact onto the PDF; moreover, the curves for $L_1 = 10$ and $L_1 = 100$ are almost identical. This is expected because the matrix W that determines the coefficients of series representations of $\tilde{H}(p|r,z)$, depends on L_1 only through the elements $B_n^{(1)}$ given by equation (A.19), in which $h_1 = L_1/R_2$ enters in the argument of $\mathrm{ctanh}(\alpha'_{n,1}h_1)$, with $\alpha'_{n,1}$ given by equation (A.10). When $\alpha'_{n,1}h_1 \geqslant \alpha'_{0,1}h_1 \gg 1$, the elements $B_n^{(1)}$ do not almost depend on h_1, implying the independence of $\tilde{H}(p|r,z)$ and thus of $H(t|r,z)$ on the height L_1, when L_1 is large enough, in agreement with panel (a). This argument is valid for any $z > 0$, i.e. when the particle starts above the pillar.

In turn, if the particle starts on a side of the pillar ($z < 0$), the dependence on L_1 is stronger because L_1 also appears in the function $s_{n,1}(z)$ given by equation (A.4). Panel (b) of figure 4 illustrates this effect for the starting point at $(r,z) = (1,0)$, i.e. at the outer reflecting boundary on the level of the pillar's top. Even here, the effect of L_1 is moderate, especially for large L_1. In the next subsection, we inspect the dependence on the height of the starting point in the case of long enough pillars.

It is worth noting that the opposite limit $L_1 \to 0$ corresponds to a periodic array of absorbing disks on the reflecting plane. Steady-state diffusion towards such configurations was studied earlier (see [48, 69–71] and references therein). For any small but strictly positive L_1, the elements $B_n^{(1)}$ behave as $R_2/(\alpha'_{n,1})^2/L_1$ for $n \ll n_0$, and as $1/\alpha'_{n,1}$ for $n \gg n_0$, where the index n_0 is determined by the condition $\alpha'_{n_0,1} \sim R_2/L_1$. As a consequence, the elements with moderate

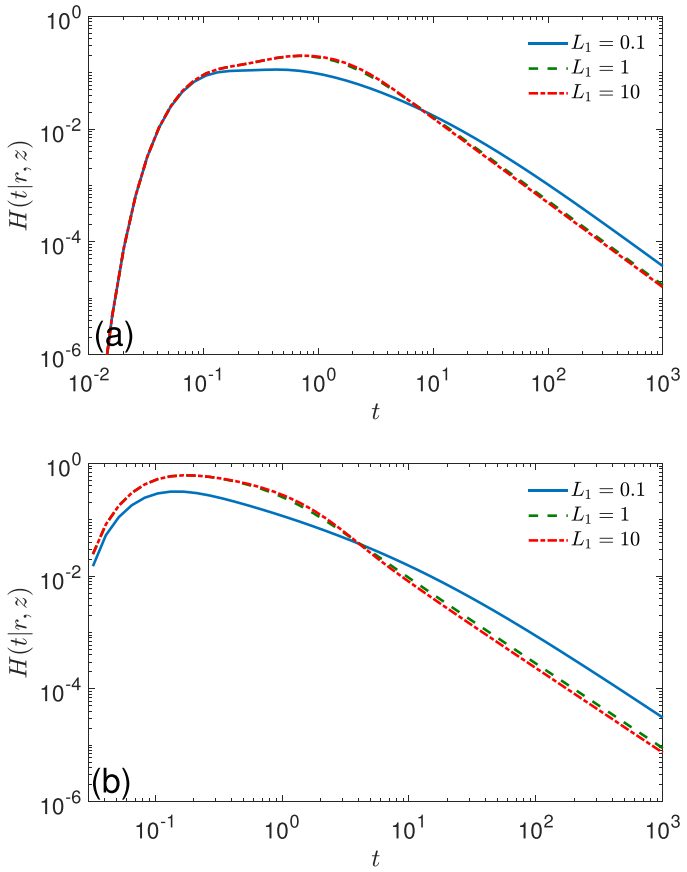

Figure 4. Probability density $H(t|r,z)$ of the FPT to the absorbing pillar, with $R_1 = 0.1$, $L_2 = 100$, three values of L_1 (see the legend), and two starting points: $r = 0$, $z = 1$ (a) and $r = 1$, $z = 0$ (b).

n are getting larger as $L_1 \to 0$, but the asymptotic form of this matrix remains unchanged. One sees that the analysis of the limit $L_1 \to 0$ is much more subtle and is beyond the scope of this paper.

3.4. Role of position z

To analyze the role of the vertical position z of the starting point, we fix the pillar's height $L_1 = 10$ and keep again $L_2 = 100$.

Figure 5 shows the PDF $H(t|r,z)$ evaluated at $r = 1$ (i.e. at the outer cylindrical boundary) and three values of z: 0, -2, and -4. Expectedly, the short-time behavior, which is determined by 'direct' trajectories and thus by the distance to the absorbing pillar, is almost identical for three cases. The long-time behavior exhibits the same power-law decay $t^{-3/2}$ but with different prefactors (we recall that the exponential cut-off due to the boundness of the domain appears at much longer times exceeding $L_2^2/D = 10^4$). When $z = 0$, one can still rely on the one-dimensional PDF $H_{1D}(t|z_0)$ from equation (16) with the offset parameter z_0 accounting for the reduced radius R_1 of the pillar (as compared to R_2). The resulting long-time asymptotic

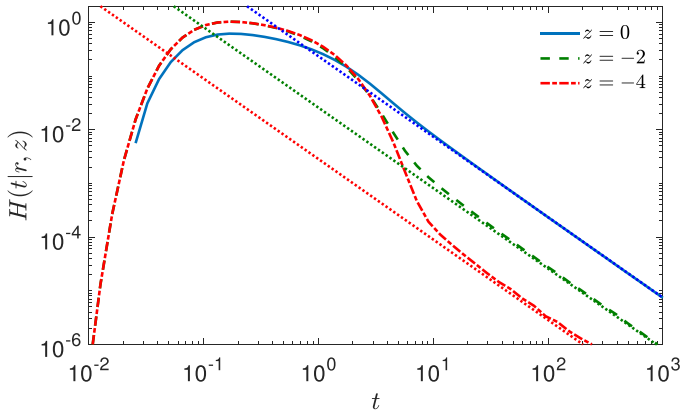

Figure 5. Probability density $H(t|r,z)$ of the FPT to the absorbing pillar, with $R_1 = 0.1$, $L_1 = 10$, $L_2 = 100$, and different locations of the starting point (r,z), with $r = 1$ and three values of z (see the legend). Three dotted lines present the long-time behavior (18), with $\alpha_{0,1} \approx 1.10$, $C(1) \approx 1.11$, and $z_0 \approx 0.75$ found in [48]. Note that the solid blue is not shown at times $t \lesssim 0.03$ due to numerical instabilities in the inversion of the Laplace transform.

behavior $z_0/\sqrt{4\pi Dt^3}$, which is shown by blue dotted line, is in excellent agreement with $H(t|r,0)$.

In order to characterize the reduced amplitude of this line for negative z, we employ the following argument. When the particle starts in the region $z<0$, one can split random trajectories in two groups: (i) those that arrived onto the pillar without crossing the level $z=0$, and (ii) those that crossed the level $z=0$. For the first group, the survival probability decays exponentially in time, with the decay time of the order of $T_1 = R_2^2/(\alpha_{0,1}^2 D)$ (see section 3.3). At times $t \gg T_1$, this contribution is negligible, and the long-time asymptotic behavior is mainly determined by the trajectories of the second group that managed to escape from the region with $z<0$ and thus can explore the elongated upper region with $z>0$. In a first approximation, the long-time behavior of $H(t|r,z)$ can thus be approximated again by $z_0/\sqrt{4\pi Dt^3}$, multiplied by the fraction of trajectories in the second group. This fraction is given by the splitting probability computed in appendix C. When $|z|/R_2$ is large enough, the splitting probability can be approximated by the leading term, see equation (C.4), so that:

$$H(t|r,z) \approx C(r)\, e^{\alpha_{0,1} z/R_2} \frac{z_0}{\sqrt{4\pi Dt^3}}, \tag{18}$$

where the amplitude $C(r)$ is defined by equation (C.5). The good accuracy of this asymptotic relation is confirmed on figure 5.

3.5. Role of radius R_1

We analyze the role of the pillar's radius R_1. When $R_1 = R_2$, the pillar fills the tube, there is no diffusion in the region $z<0$, while the survival probability for the upper region $z>0$ is simply given by $S_{1D}(t|z)$ for diffusion on the interval $(0,L_2)$, see equation (B.1). When R_1 is smaller but still comparable to R_2, the particle that managed to enter the region $z<0$, is rapidly absorbed by the side surface of the pillar. In this light, configurations with long but thin pillar (i.e. $R_1 \ll R_2$) seem to be most interesting from both theoretical and practical points of view.

In the limit $\rho = R_1/R_2 \to 0$, the pillar shrinks to a needle, i.e. a finite segment or a half-line, which are 'invisible' for Brownian motion [72]. In other words, an infinitely thin pillar cannot absorb the particle, and the survival probability is equal to 1 in this limit. However, the approach to this limit is very slow. As discussed in [48], the asymptotic behavior of Bessel functions implies that:

$$\alpha_{0,1} \approx \frac{\sqrt{2}}{\sqrt{\ln(1/\rho) - 3/4}} \quad (\rho \to 0). \tag{19}$$

One sees that $\alpha_{0,1}$ indeed vanishes as $\rho \to 0$ but extremely slowly. In particular, this slow decay ensures that the decay time $R_2^2/(\alpha_{0,1}^2 D)$ associated to planar diffusion is generally (much) smaller than the decay time $4L_2^2/(\pi^2 D)$ associated to diffusion in the upper region when $L_2/R_2 \gg 1$. In fact, this occurs when:

$$\frac{L_2}{R_2} > \frac{\pi}{2\sqrt{2}} \sqrt{\ln(1/\rho) - 3/4}\,. \tag{20}$$

For instance, if $\rho = 10^{-2}$, this inequality leads to a moderate constraint $L_2/R_2 > 2.18$. Alternatively, one can get a bound on the relative radius of the pillar:

$$\rho > \exp\bigl(-3/4 - (8/\pi^2)(L_2/R_2)^2\bigr). \tag{21}$$

Even for a moderate value $L_2/R_2 = 5$, the decay time associated to one-dimensional diffusion is dominant whenever the relative radius exceeds 7.5×10^{-10}, i.e. in any relevant setting.

3.6. Role of proximity to the pillar

In previous sections, the starting point was located relatively far from the pillar, with the distance to the pillar being equal to R_2. Let us now look at the effect of proximity of the starting point to the pillar.

If the particle is released from a point (r, z) near the top of the pillar (i.e. $0 < z \ll R_1$ and $r \ll R_1$), the particle explores at short times the vicinity of a flat boundary, as it was near an absorbing plane in the upper half-space. As a consequence, the PDF of the FPT is accurately described by $H_{1D}(t|z)$ from equation (16). As time increases, the particle starts to 'feel' that the top of the pillar has a finite radius, and thus deviates from equation (16). Note that if L_2 is large enough, the long-time behavior is again one-dimensional and given by $H_{1D}(t|z + z_0)$, which exhibits the same long-time $t^{-3/2}$ behavior but with a higher amplitude (see section 3.2).

Let us now examine another setting when the particle is released from a point (r, z) near the side of the pillar (i.e. $R_1 < r \ll R_2$ and $z < 0$ with $|z| \gg R_2$). At short times, the particle explores a vicinity of the curved surface of a cylindrical pillar of radius R_1, as if it diffused outside an infinite absorbing cylinder of radius R_1 in the three-dimensional space. This is equivalent to planar diffusion outside an absorbing circle of radius R_1 (at this time, diffusion along the z axis does not matter yet). In this case, the survival probability is known to exhibit a very slow decay (see, e.g. [73–75]):

$$S_{2D}(t|r) \approx \frac{2\ln(r/R_1)}{\ln(Dt/R_1^2)} \quad (t \to \infty), \tag{22}$$

from which:

$$H_{2D}(t|r) \approx \frac{2\ln(r/R_1)}{t[\ln(Dt/R_1^2)]^2} \quad (t \to \infty). \tag{23}$$

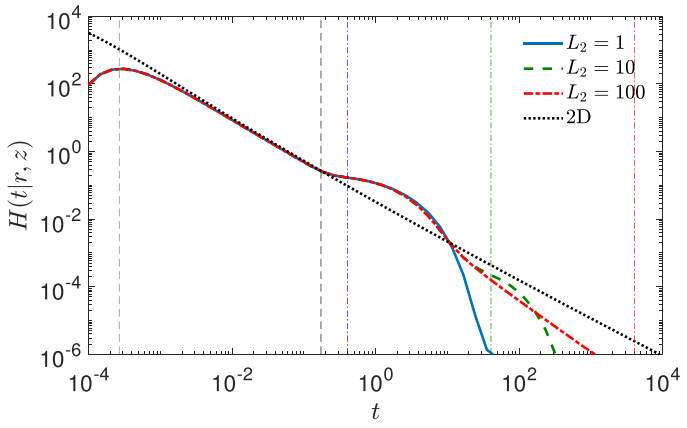

Figure 6. Probability density $H(t|r,z)$ of the FPT to the absorbing pillar, with $R_1 = 0.01$, $L_1 = 10$, $(r,z) = (0.05,-2)$, and three values of L_2 (see the legend). Dotted line presents the long-time behavior (24) for planar diffusion. Vertical dashed lines indicate several time scales: $(r-R_1)^2/(6D) \approx 2.7\times 10^{-4}$ is the most probable FPT, $R_2^2/(j_{0,1}^2 D) \approx 0.17$ is the decay time for planar diffusion towards an absorbing disk of radius R_2, where $j_{0,1} \approx 2.4048$ is the first positive zero of $J_0(z)$, while $4\times 1^2/(\pi^2 D) \approx 0.4$, $4\times 10^2/(\pi^2 D) \approx 40$ and $4\times 100^2/(\pi^2 D) \approx 4000$ are the decay times for one-dimensional diffusion with $L_2 = 1, 10$ and 100, respectively.

A more accurate expression for the asymptotic behavior of the PDF was given in [44, 76]

$$H_{2D}(t|r) \approx \frac{2\ln(r/R_1)}{t\left[\pi^2 + \left(\ln(R_1^2/(4Dt)) + 2\gamma\right)^2\right]}, \tag{24}$$

where $\gamma \approx 0.5772$ is the Euler constant. Note that the integral of this expression yields:

$$S_{2D}(t|r) \approx \frac{2\ln(r/R_1)}{\pi} \arctan\left(\frac{\pi}{\ln(4Dt/R_1^2) - 2\gamma}\right). \tag{25}$$

At very large t, one retrieves equations (22) and (23).

These expressions provide the long-time asymptotic behavior for planar diffusion outside an absorbing circle. In our case, however, these expressions yield the transient behavior at intermediate time scales, until the particle starts to 'feel' the confinement. As time increases further, the motion of the particle is affected by confinement, and the asymptotic behavior changes. This change occurs at the time needed to reach the outer boundary of radius R_2. The latter can be estimated as the decay time $T_2 = R_2^2/(j_{0,1}^2 D) \approx 0.17$ of the survival probability of a particle diffusing inside a disk of radius R_2 with the absorbing boundary, where $j_{0,1} \approx 2.4048$ is the first positive zero of the Bessel function $J_0(z)$. At even longer times, the particle may reach the upper region (with $z > 0$) and diffuse further away from the pillar. If L_2 is large enough, another intermediate regime with the $t^{-3/2}$ decay is established, as discussed in section 3.2. This regime is terminated by an exponential cut-off with the decay time T discussed in section 3.1.

Figure 6 illustrates the effect of proximity of the starting point to the pillar's side. Here we consider a thin pillar ($R_1 = 0.01$) and locate the starting point (r,z) close to the pillar's boundary at $r = 0.05$ and $z = -2$. At short times, at which the particle does not 'feel' the presence of the outer reflecting boundary, one retrieves the asymptotic behavior (24) reminiscent of planar diffusion. At the time scale T_2 shown by a black dashed vertical line, there appear deviations

from equation (24). At even longer times, one observes another intermediate regime with the $t^{-3/2}$ decay, which corresponds to a diffusive exploration of the upper region (with $z>0$). This regime is terminated by an exponential cut-off at the time decay $4L_2^2/(\pi^2 D)$ for one-dimensional diffusion, which is equal to 0.4, 40 and 4000 at $L_2 = 1, 10$, and 100, respectively. Clearly, this time scale for $L_2 = 1$ is too close to $T_2 \approx 0.17$ so that the intermediate regime does not exist. In turn, it is clearly visible at $L_2 = 100$.

3.7. Comparison with the self-consistent approximation

In [44], the distribution of the FPT was studied for a similar configuration of two coaxial cylinders of radii R_1 and R_2, capped by the parallel planes at $z = -L_1$ and $z = L_2$. The absorbing region was located on a lower part ($-L_1 < z < 0$) of the inner cylinder, while its upper part ($0 < z < L_2$) was reflecting. While this configuration resembles our setting with an absorbing pillar, there is a significant difference: the upper inner cylinder was impenetrable to diffusing particles so that the top of the pillar was inaccessible in [44]. When the inner cylinder is very thin, such a difference does not seem to be significant. In contrast, if the inner cylinder is moderately thin, the excluded volume may play an important role. In particular, the top of the pillar may have very high chances to absorb the particle arriving from a remote point above the pillar, thus screening the side of the pillar. Note also that the limit $L_1 \to 0$ is totally different in two settings: in our case, the pillar shrinks to a disk, which can still absorb particles; in turn, in the setting of [44], the absorbing region was exclusively located on the side of the pillar, and the survival probability becomes equal to 1 in the limit $L_1 \to 0$. We conclude that our study provides complementary insights onto diffusion-controlled reactions in such domains.

4. Conclusion

In this paper, we investigated the distribution of the FPT to a periodic array of absorbing pillars confined between two parallel reflecting planes. The replacement of a periodic cell of the original system by a cylindrical tube with reflecting boundary that englobes a single pillar allowed us to solve exactly the modified Helmholtz equation in cylindrical coordinates. For this purpose, we adopted the mode matching method that we recently developed for studying steady-state diffusion governed by the Laplace equation [48]. In this way, we managed to obtain an exact representation of the Laplace-transformed PDF $\tilde{H}(p|r,z)$ of the FPT. Despite the need for a numerical inversion of a truncated matrix with explicitly known elements, this solution presents many advantages: (i) analytical dependence of $\tilde{H}(p|r,z)$ on the starting point (r,z); (ii) rapid convergence and therefore very fast numerical computation; (iii) identification of respective roles of different geometric parameters onto the solution; and (iv) asymptotic analysis. In particular, the method was fast enough to undertake an inverse Laplace transform numerically and to get the survival probability $S(t|r,z)$ and the PDF $H(t|r,z)$ in time domain.

From a theoretical point of view, an absorbing pillar surrounded by a reflecting boundary is a rich geometric model to investigate various aspects of the FPT distribution. In fact, former theoretical studies were focused on simpler geometric settings like coaxial cylinders or concentric spheres. In turn, the current model has four geometric parameters: the pillar's height L_1 and radius R_1, the distance L_2 to the upper plane, and the radius R_2 of the outer reflecting boundary (which is also related to the inter-pillar distance in the original periodic array of pillars). As a consequence, different asymptotic regimes can emerge and even co-exist. For instance, figure 6 presented the PDF with four distinct regimes: (i) a universal short-time behavior $e^{-(r-R_1)^2/(4Dt)}/t^{3/2}$ governed by 'direct trajectories' (left tail), an intermediate behavior

$1/(t\ln^2(Dt/R_1^2))$ due to effectively planar diffusion, an intermediate behavior $t^{-3/2}$ due to effectively one-dimensional exploration of the upper region, and a universal exponential cut-off $e^{-t/T}$ due to confinement. Even though each of these regimes have been studied in the past, we are unaware of earlier observations of all these features in a single PDF. In order to better understand these features, we discussed how different geometric parameters affect the distribution.

From a practical point of view, spiky coatings have recently drown significant attention due to the rapid progress in fabrication technology and favorable performance in many applications [77] such as superhydrophobic materials [78], filtration [79, 80], sensing systems [81, 82], selective protein separation [83], to name but a few. At the same time, a theoretical description of their trapping efficiency was still missing, especially in a transient time-dependent regime. To our knowledge, this is the first study of the FPT in such structures. We stress that the derived exact solution goes far beyond the conventional mean FPT, which is uninformative and actually misleading if the upper plane is located far away from the pillars. We therefore expect that the presented method and solution may guide experimentalists in the intelligent design of spiky coatings with desired trapping properties.

Data availability statement

No new data were created or analysed in this study.

Acknowledgments

D S G acknowledges the Alexander von Humboldt Foundation for support within a Bessel Prize award. A T S thanks Paul A Martin for many illuminating discussions.

Appendix A. Exact solution

In this appendix, we provide the details of the derivation of the exact solution of the boundary value problem (3). This derivation closely follows the appendix of [48], in which the mode matching method was used to solve the Laplace equation. Even though many notations and equations are identical, we reproduce the whole derivation to highlight subtle modifications that are required for solving the modified Helmholtz equation (3a).

A.1. Derivation of the solution

Due to the axial symmetry, the boundary value problem (3) is actually a two-dimensional problem in an L-shape region (see figure 1(c)). Note that one has to add the Neumann boundary condition,

$$\partial_r \tilde{H} = 0 \quad (r = 0,\ 0 < z < L_2), \tag{A.1}$$

to account for the regularity and axial symmetry of the problem. One can search for its solution separately in two rectangular subdomains, $\Omega_1 = (R_1, R_2) \times (-L_1, 0)$ and $\Omega_2 = (0, R_2) \times (0, L_2)$, and then match them at the junction interval (at $z = 0$).

A general solution in Ω_1 reads:

$$\tilde{H}(p|r,z) = w(r/R_2) - \sum_{n=0}^{\infty} c_{n,1}\, v_{n,1}(r/R_2)\, s_{n,1}(z)\,, \tag{A.2}$$

with unknown coefficients $c_{n,1}$, where:

$$w(\bar{r}) = \frac{K_1(\alpha)I_0(\alpha\bar{r}) + I_1(\alpha)K_0(\alpha\bar{r})}{K_1(\alpha)I_0(\alpha\rho) + I_1(\alpha)K_0(\alpha\rho)}, \tag{A.3}$$

with $\alpha = R_2\sqrt{p/D}$, $\rho = R_1/R_2$, $\bar{r}$ denoting dimensionless radius,

$$s_{n,1}(z) = \frac{\cosh(\alpha'_{n,1}(L_1+z)/R_2)}{\cosh(\alpha'_{n,1}L_1/R_2)} \tag{A.4}$$

and

$$v_{n,1}(\bar{r}) = e_n w_n(\bar{r}), \tag{A.5}$$

with

$$w_n(\bar{r}) = J_1(\alpha_{n,1})Y_0(\alpha_{n,1}\bar{r}) - Y_1(\alpha_{n,1})J_0(\alpha_{n,1}\bar{r}), \tag{A.6}$$

and we used $J_0'(z) = -J_1(z)$, $Y_0'(z) = -Y_1(z)$, prime denotes the derivative, $J_\nu(z)$ and $Y_\nu(z)$ are the Bessel functions of the first and second kind, respectively, and $I_\nu(z)$ and $K_\nu(z)$ are the modified Bessel functions. The prefactor:

$$e_n = \frac{\sqrt{2}}{\sqrt{[w_n(1)]^2 - \rho^2[w_n'(\rho)/\alpha_{n,1}]^2}} \tag{A.7}$$

ensures the normalization of the radial function $v_{n,1}(\bar{r})$:

$$\int_\rho^1 \mathrm{d}\bar{r}\,\bar{r}\,[v_{n,1}(\bar{r})]^2 = 1, \tag{A.8}$$

where we used:

$$\int_\rho^1 \mathrm{d}\bar{r}\,\bar{r}\,w_n^2(\bar{r}) = \frac{1}{2\alpha_{n,1}^2}\left(\bar{r}^2[w_n'(\bar{r})]^2 + \alpha_{n,1}^2\bar{r}^2[w_n(\bar{r})]^2\right)_\rho^1 = \frac{[w_n(1)]^2 - \rho^2[w_n'(\rho)/\alpha_{n,1}]^2}{2},$$

with $w_n(\rho) = 0$ and $w_n'(1) = 0$ being employed. By construction, $\tilde{H}(p|r,z)$ from equation (A.2) satisfies equations (3*a*), (3*f*) and (3*e*). The parameters $\alpha_{n,1}$ are obtained by imposing the condition (3*c*) at $r = R_1$ (i.e. setting $w_n(\rho) = 0$) and solving the resulting equation:

$$Y_1(\alpha_{n,1})J_0(\alpha_{n,1}\rho) - J_1(\alpha_{n,1})Y_0(\alpha_{n,1}\rho) = 0. \tag{A.9}$$

This equation has infinitely many positive solutions $\{\alpha_{n,1}\}$, which are enumerated by $n = 0,1,2,\ldots$ in an increasing order [84]. As $\{v_{n,1}(\bar{r})\}$ are the eigenfunctions of the differential operator $\partial_r^2 + (1/r)\partial_r$, they form a complete orthonormal basis in the space $L_2(\rho,1)$ of r-weighted square-integrable functions on $(\rho,1)$. Finally, one sets:

$$\alpha'_{n,1} = \sqrt{\alpha_{n,1}^2 + R_2^2 p/D}. \tag{A.10}$$

A general solution in Ω_2 reads:

$$\tilde{H}(p|r,z) = \sum_{n=0}^{\infty} c_{n,2}\, v_{n,2}(r/R_2)\, s_{n,2}(z), \tag{A.11}$$

with unknown coefficients $c_{n,2}$, where:

$$v_{n,2}(\bar{r}) = \frac{J_0(\alpha_{n,2}\bar{r})}{J_0(\alpha_{n,2})}, \tag{A.12}$$

and

$$s_{n,2}(z) = \frac{\cosh(\alpha'_{n,2}(L_2 - z)/R_2)}{\cosh(\alpha'_{n,2}L_2/R_2)}\,. \tag{A.13}$$

By construction, $\tilde{H}(p|r,z)$ from equation (A.11) satisfies equations (3*a*), (3*d*) and (A.1). The parameters $\{\alpha_{n,2}\}$ are obtained by imposing the condition (3*f*), which reads as:

$$J_1(\alpha_{n,2}) = 0 \quad (n = 0,1,2,\ldots). \tag{A.14}$$

This equation has infinitely many positive solutions $\{\alpha_{n,2}\}$, which are enumerated by $n = 0,1,2,\ldots$ in an increasing order [84]. The prefactor in equation (A.12) ensures the normalization:

$$\int\limits_0^1 \mathrm{d}\bar{r}\,\bar{r}\,[v_{n,2}(\bar{r})]^2 = \frac{1}{2}\,. \tag{A.15}$$

As $\{\sqrt{2}\,v_{n,2}(\bar{r})\}$ are the eigenfunctions of the differential operator $\partial_r^2 + (1/r)\partial_r$, they form a complete orthonormal basis in the space $L_2(0,1)$. Finally, one sets:

$$\alpha'_{n,2} = \sqrt{\alpha_{n,2}^2 + R_2^2 p/D}. \tag{A.16}$$

Note that $\alpha_{0,2} = 0$ so that $\alpha'_{0,2} = \alpha$.

The unknown coefficients $c_{n,1}$ and $c_{n,2}$ are then determined by matching the representations (A.2) and (A.11) at $z = 0$, i.e. by requiring the continuity of $\tilde{H}(p|r,z)$ and of its derivative $\partial_z\tilde{H}(p|r,z)$. The second condition, which should be satisfied for any $R_1 < r < R_2$, reads:

$$R_2(\partial_z\tilde{H})_{z=0^-} = \sum_{n=0}^{\infty} \tilde{c}_{n,1} v_{n,1}(r/R_2) = \sum_{n=0}^{\infty} \tilde{c}_{n,2} v_{n,2}(r/R_2) = R_2(\partial_z\tilde{H})_{z=0^+}\,, \tag{A.17}$$

where

$$\tilde{c}_{n,1} = \frac{c_{n,1}}{B_n^{(1)}}\,, \qquad \tilde{c}_{n,2} = -c_{n,2}B_n^{(2)}, \tag{A.18}$$

and

$$B_n^{(1)} = \frac{1}{R_2 s'_{n,1}(0)} = \frac{\mathrm{ctanh}(\alpha'_{n,1}L_1/R_2)}{\alpha'_{n,1}}\,, \tag{A.19}$$

$$B_n^{(2)} = -R_2 s'_{n,2}(0) = \alpha'_{n,2}\tanh(\alpha'_{n,2}L_2/R_2), \tag{A.20}$$

with $\tanh(z)$ and $\mathrm{ctanh}(z)$ denoting the hyperbolic tangent and cotangent functions, respectively. Multiplying equation (A.17) by $\bar{r}\,v_{k,1}(\bar{r})$ and integrating from ρ to 1, one gets:

$$\sum_{n=0}^{\infty} \tilde{c}_{n,2} \int\limits_{\beta}^{1} \mathrm{d}\bar{r}\,\bar{r}\,v_{k,1}(\bar{r})\,v_{n,2}(\bar{r}) = \tilde{c}_{k,1}$$

due to orthogonality of $\{v_{k,1}(\bar{r})\}$. Setting,

$$A_{k,n} = \int\limits_{\rho}^{1} \mathrm{d}\bar{r}\,\bar{r}\,v_{k,1}(\bar{r})\,v_{n,2}(\bar{r}), \tag{A.21}$$

we can rewrite the above equations as:

$$c_{k,1} = B_k^{(1)} \sum_{n=0}^{\infty} A_{k,n} B_n^{(2)} c_{n,2} \,. \tag{A.22}$$

Moreover, as the radial functions $v_{k,1}(\bar{r})$ and $v_{k,2}(\bar{r})$ are linear combinations of Bessel functions of the same order, the integral in equation (A.21) can be found explicitly:

$$A_{k,n} = \left(\bar{r} \frac{v_{k,1}(\bar{r}) v'_{n,2}(\bar{r}) - v'_{k,1}(\bar{r}) v_{n,2}(\bar{r})}{\alpha_{k,1}^2 - \alpha_{n,2}^2} \right)_{\bar{r}=\rho}^{1} = \frac{\rho\, v'_{k,1}(\rho)\, v_{n,2}(\rho)}{\alpha_{k,1}^2 - \alpha_{n,2}^2} \,, \tag{A.23}$$

where we used the boundary conditions $v_{k,1}(\rho) = v'_{k,1}(1) = v'_{n,2}(1) = 0$.

Similarly, we impose the continuity of the function $\tilde{H}(p|r,z)$ at $z = 0$, together with equation (3*b*):

$$\tilde{H}(p|r,0^+) = \begin{cases} 1 & (0 < r < R_1), \\ \tilde{H}(p|r,0^-) & (R_1 < r < R_2). \end{cases} \tag{A.24}$$

Multiplying this relation by $\bar{r} v_{k,2}(\bar{r})$ and integrating from 0 to 1, we get:

$$\frac{c_{k,2}}{2} = -\frac{\rho v'_{k,2}(\rho)}{\alpha_{k,2}^2} + \int_{\rho}^{1} \mathrm{d}\bar{r}\, \bar{r}\, v_{k,2}(\bar{r})\, w(\bar{r}) - \sum_{n=0}^{\infty} c_{n,1} A_{n,k}, \tag{A.25}$$

where we used the orthogonality of functions $\{v_{k,2}(\bar{r})\}$ and their normalization (A.15); note that the first term is equal to $\rho^2/2$ for $k = 0$. Substituting $c_{n,1}$ from equation (A.22), we get:

$$c_{k,2} + 2 \sum_{n=0}^{\infty} A_{n,k} B_n^{(1)} \sum_{n'=0}^{\infty} A_{n,n'} B_{n'}^{(2)} c_{n',2} = V_k \,, \tag{A.26}$$

where

$$\frac{V_k}{2} = -\frac{\rho v'_{k,2}(\rho)}{\alpha_{k,2}^2} + \int_{\rho}^{1} \mathrm{d}\bar{r}\, \bar{r}\, v_{k,2}(\bar{r}) w(\bar{r}). \tag{A.27}$$

In analogy to equation (A.23), one can compute the second integral explicitly:

$$\begin{aligned} \frac{V_k}{2} &= -\frac{\rho v'_{k,2}(\rho)}{\alpha_{k,2}^2} + \left(\bar{r} \frac{v_{k,2}(\bar{r}) w'(\bar{r}) - v'_{k,2}(\bar{r}) w(\bar{r})}{\alpha_{k,2}^2 + \alpha^2} \right)_{\bar{r}=\rho}^{1} \\ &= -\frac{\rho v'_{k,2}(\rho)}{\alpha_{k,2}^2} - \rho \frac{v_{k,2}(\rho)\, w'(\rho) - v'_{k,2}(\rho)}{\alpha_{k,2}^2 + \alpha^2} \,, \end{aligned} \tag{A.28}$$

where we used that $w(\rho) = 1$. It is convenient to re-arrange two sums in equation (A.25) as:

$$c_{k,2} + \sum_{n=0}^{\infty} W_{k,n}\, c_{n,2} = V_k \quad (k = 0, 1, 2, \ldots), \tag{A.29}$$

where

$$W_{k,n} = 2 \sum_{n'=0}^{\infty} A_{n',k} B_{n'}^{(1)} A_{n',n} B_n^{(2)} \,, \tag{A.30}$$

i.e. we got the infinite system of linear algebraic equations for the unknown coefficients $c_{k,2}$ with $k = 0, 1, 2, \ldots$. To compute these coefficients, one needs to construct the infinite-dimensional matrix W and then to invert the matrix $I + W$, where I is the identity matrix. In practice, one can truncate the matrix $I + W$ to a finite size $N \times N$ and then perform the inversion numerically. Once the coefficients $c_{n,2}$ are found, one can determine $c_{n,1}$ according to equation (A.22). This completes the construction of the exact solution of the problem (3). Even though this construction involves numerical inversion of the truncated matrix, the obtained expressions (A.2) and (A.11) provides an explicit analytical dependence of $\tilde{H}(p|r,z)$ on r and z via the functions $v_n(r/R_2)$ and $s_n(z)$. Moreover, the accuracy of the numerical computation of $\tilde{H}(p|r,z)$ rapidly improves as the truncation order N increases. In most cases, one can use moderate values of N (say, few tens) to get very accurate results.

Importantly, the structure of the exact solution reveals how different geometric parameters can affect the FPT distribution: the pillar height L_1 enters only via $B_n^{(1)}$, the distance to the source L_2 enters only via $B_n^{(2)}$, so that the matrix A does not depend on L_1 and L_2. Similarly, the matrix A does not depend on p. These properties can be used for deriving various asymptotic behaviors (see, e.g. appendix A.3). For instance, in the limit $p \to 0$, one has $w(\bar{r}) \to 1$ and $w'(\rho) \approx (\rho - 1/\rho)\alpha^2/2$. As a consequence, one gets:

$$\frac{V_k}{2} \approx -\rho \frac{v_{k,2}(\rho) w'(\rho)}{\alpha_{k,2}^2} \to 0 \qquad (k > 0), \tag{A.31}$$

whereas $V_0 \to 1$. Moreover, one has $B_0^{(2)} \to 0$ so that $W_{k,0} \to 0$. In this limit, one deals with the homogeneous system of linear equations,

$$c_{k,2} + \sum_{n=1}^{\infty} W_{k,n} c_{n,2} = 0 \qquad (k = 1, 2, \ldots), \tag{A.32}$$

which has the trivial solution $c_{k,2} = 0$ for all $k > 0$. In addition, one gets $c_{0,2} = 1$ and therefore retrieves the expected normalization:

$$\int_0^{\infty} \mathrm{d}t H(t|r,z) = \tilde{H}(0|r,z) = 1. \tag{A.33}$$

A.2. Averages over the starting point

In some applications, the precise location of the starting point is unknown or irrelevant, and it is convenient to average the survival probability and the PDF of the FPT as if the starting point was uniformly distributed.

First, we consider the average over a cross section at a given height z. We get

$$\overline{\tilde{H}_1}(z) = \frac{2\pi}{\pi (R_2^2 - R_1^2)} \int_{R_1}^{R_2} \mathrm{d}r r \tilde{H}(p|r,z) = -\frac{2\rho}{1-\rho^2} \left(\frac{w'(\rho)}{\alpha^2} + \sum_{n=0}^{\infty} c_{n,1} s_{n,1}(z) \frac{v'_{n,1}(\rho)}{\alpha_{n,1}^2} \right) \quad (z < 0), \tag{A.34}$$

and

$$\overline{\tilde{H}_2}(z) = \frac{2\pi}{\pi R_2^2} \int_0^{R_2} \mathrm{d}r r \tilde{H}(p|r,z) = c_{0,2} \frac{\cosh((L_2 - z)\sqrt{p/D})}{\cosh(L_2\sqrt{p/D})} \quad (z > 0), \tag{A.35}$$

where we used:

$$\int_\rho^1 \mathrm{d}\bar{r}\,\bar{r}\,v_{n,1}(\bar{r}) = \frac{\rho\, v'_{n,1}(\rho)}{\alpha^2_{n,1}} \tag{A.36}$$

due to the boundary conditions (and similar equation holds for the integral of $\bar{r}w(\bar{r})$), and $\alpha'_{0,2} = \alpha = R_2\sqrt{p/D}$. One sees that the coefficient $c_{0,2}$ can thus be interpreted as the cross-sectional average of $\tilde{H}(p|r,z)$ at $z=0$. In addition,

$$\overline{\tilde{H}_1}(-L_1) = -\frac{2\rho}{1-\rho^2}\left(\frac{w'(\rho)}{\alpha^2} + \sum_{n=0}^{\infty} \frac{c_{n,1}}{\cosh(\alpha'_{n,1}L_1/R_2)}\frac{v'_{n,1}(\rho)}{\alpha^2_{n,1}}\right) \tag{A.37}$$

corresponds to the setting when the particle is released from the bottom surface and has high chances to be absorbed by the pillar; the knowledge of the PDF allows one to quantify an escape from the nanoforest of absorbing pillars. When L_1/R_2 is large (i.e. the pillars are high), the sum can be neglected, and one retrieves the surface-averaged Laplace-transformed PDF in an annulus between an absorbing inner circle and a reflecting outer circle. In contrast, if the particle is released from the top surface, $\overline{\tilde{H}_2}(L_2)$ characterizes how efficiently the nanoforest of absorbing pillars can capture such a particle diffusing from a remote location.

Second, we can use these expressions to compute the volume average, as if the starting point was uniformly distributed in the bulk:

$$\begin{aligned}\overline{\tilde{H}} &= \frac{1}{\pi\left(R_2^2 - R_1^2\right)L_1 + \pi R_2^2 L_2}\left(\pi\left(R_2^2 - R_1^2\right)\int_{-L_1}^{0}\mathrm{d}z\overline{\tilde{H}_1}(z) + \pi R_2^2\int_0^{L_2}\mathrm{d}z\overline{\tilde{H}_2}(z)\right)\\ &= \frac{1}{(1-\rho^2)h_1 + h_2}\left(-2\frac{\rho w'(\rho)}{\alpha^2}h_1 - 2\sum_{n=0}^{\infty}c_{n,1}\frac{\rho v'_{n,1}(\rho)}{\alpha^2_{n,1}}\frac{\tanh(\alpha'_{n,1}h_1)}{\alpha'_{n,1}} + c_{0,2}\frac{\tanh(\alpha h_2)}{\alpha}\right),\end{aligned}$$

where $h_1 = L_1/R_2$ and $h_2 = L_2/R_2$.

A.3. Long-time behavior in the limit $L_2 = \infty$

In this section, we discuss the long-time behavior of the PDF $H(t|r,z)$ in the configuration with $L_2 = \infty$. We recall that L_2 affects the coefficients $c_{n,1}$ and $c_{n,2}$ of the Laplace-transformed PDF $\tilde{H}(p|r,z)$ only through the matrix elements $B_n^{(2)}$ given by equation (A.20). As the long-time behavior of $H(t|r,z)$ corresponds to the small-p behavior of $\tilde{H}(p|r,z)$, it is instructive to look at the behavior of $B_n^{(2)}$ as $p\to 0$. For $n>0$, $\alpha'_{n,2}\to\alpha_{n,2}>0$, with $O(p)$ corrections, so that the elements $B_n^{(2)}$ tend to strictly positive limits. In contrast, $\alpha'_{0,2} = \alpha = R_2\sqrt{p/D}\to 0$, and the asymptotic behavior of $B_0^{(2)}$ depends on whether L_2 is finite or not:

$$B_0^{(2)} \approx \begin{cases} L_2/R_2 & (L_2<\infty)\\ \alpha & (L_2=\infty)\end{cases} \qquad (p\to 0). \tag{A.38}$$

We start with the case $L_2=\infty$. According to the definition (A.30), the matrix $I+W$ can be written as:

$$I + W \approx I + W_0 + \alpha Y + O(p), \tag{A.39}$$

where W_0 denotes the matrix W evaluated at $p=0$, and the matrix Y has the elements:

$$Y_{k,n} = 2\delta_{n,0} \sum_{n'=0}^{\infty} A_{n',k} B_{n'}^{(1)} A_{n',0}\,, \tag{A.40}$$

i.e. it has only one nonzero column at $n=0$. The coefficients $c_{n,2}$ can then be found as:

$$c_{n,2} = \big[(I+W)^{-1}V\big]_n \approx \Big[(I+W_0)^{-1} - \alpha(I+W_0)^{-1}Y(I+W_0)^{-1} + O(p)\Big]_n .$$

Substituting these coefficients into equation (A.11), one gets:

$$\tilde{H}(p|r,z) = 1 - C\sqrt{p/D} + O(p), \tag{A.41}$$

where the constant term comes from the normalization, while the subleading term is of the order of $p^{1/2}$, with some prefactor C (this prefactor can be expressed from the above formulas). This asymptotic behavior implies $\tilde{S}(p|r,z) \approx C/\sqrt{pD}$, from which the Tauberian theorem yields the long-time behaviors:

$$S(t|r,z) \approx \frac{C}{\sqrt{\pi D t}} \quad \Rightarrow \quad H(t|r,z) \approx \frac{C}{\sqrt{4\pi D t^3}}\,. \tag{A.42}$$

The above 'derivation' does not pretend to be mathematically rigorous; in fact, one deals here with infinite-dimensional matrices that requires a more refined analysis, in particular, on the convergence. Nevertheless, this derivation highlights the emergence of the $p^{1/2}$-contribution from the matrix element $B_0^{(2)}$ as the mathematical origin of the slow power-law decay. In fact, if L_2 is finite, $B_0^{(2)} \to L_2/R_2$, and there is no $p^{1/2}$-term. In this case, one would simply get $\tilde{H}(p|r,z) = 1 + O(p)$, and the coefficient in front of $-p$ would be the mean FPT. Moreover, the analysis of the poles (see appendix A.4) would yield the exponential decay of $H(t|r,z)$, in sharp contrast to equation (A.42) for $L_2 = \infty$.

Note that the situation is different in the limit $L_1 \to \infty$ (with a finite L_2). Here, the height L_1 affects the coefficients $c_{n,1}$ and $c_{n,2}$ through the matrix elements $B_n^{(1)}$, which involve $\alpha'_{n,1}$ that approach strictly positive limits $\alpha_{n,1}$ as $p \to 0$ for all n. As a consequence, the $p^{1/2}$-terms do not emerge, and the mean FPT remains finite, regardless whether L_1 is finite or infinite.

A.4. Poles

The poles of the Laplace-transformed survival probability $\tilde{S}(p|r,z)$ determine the eigenvalues λ_n of the Laplace operator in the considered domain. As discussed in the text, the eigenvalues are strictly positive so that all the poles lie on the negative axis in the complex plane $p \in \mathbb{C}$. At each pole, the matrix $I+W$ determining the coefficients $c_{n,2}$ is not invertible, i.e. its determinant is zero: $\det(I+W) = 0$. This equation can be used for a numerical computation of the poles. However, the computation is rather subtle because the matrix W, which was originally constructed for positive p, is divergent at some negative values of p. We recall that the matrix W depends on p through two diagonal matrices $B^{(1)}$ and $B^{(2)}$ whose elements are given by equations (A.19) and (A.20). As these elements involve respectively $\mathrm{ctanh}(\alpha'_{n,1}h_1)$ and $\tanh(\alpha'_{n,2}h_2)$ (with $h_1 = L_1/R_2$ and $h_2 = L_2/R_2$), they become infinite when $\alpha'_{n,1}h_1 = i\pi k$ or $\alpha'_{n,2}h_2 = i(\pi/2 + \pi k)$, for any integer k. In other words, there are two families of points,

$$\frac{R_2^2}{D} p_{n,k}^{(1)} = -\frac{\pi^2 k^2}{h_1^2} - \alpha_{n,1}^2 \quad \begin{pmatrix} n=0,1,2,\dots \\ k=0,1,2,\dots \end{pmatrix}, \tag{A.43a}$$

$$\frac{R_2^2}{D} p_{n,k}^{(2)} = -\frac{\pi^2 (k+1/2)^2}{h_2^2} - \alpha_{n,2}^2 \quad \begin{pmatrix} n=0,1,2,\dots \\ k=0,1,2,\dots \end{pmatrix}, \tag{A.43b}$$

at which $\det(I+W)$ is infinite. By ordering these points, one can search for the poles (i.e. the zeros of $\det(I+W)$) on intervals between each pair of these consecutive points. These points actually help to locate the poles. Moreover, they can also be used to get upper and lower bounds on each pole. For instance, the pole p_0 determining the principal eigenvalue λ_0 is bounded by:

$$0 < |p_0| \leqslant \min\{|p_{0,0}^{(1)}|, |p_{0,0}^{(2)}|\} = \min\left\{\frac{\alpha_{0,1}^2 D}{R_2^2}, \frac{\pi^2 D}{4L_2^2}\right\}, \tag{A.44}$$

in agreement with the bound (11).

A.5. Thin pillar asymptotic behavior

In this section, we briefly discuss the limit $R_1 \to 0$, which affects the solutions $\alpha_{n,1}$ of equation (A.9) and thus the matrix elements of A and $B^{(1)}$. Following a similar analysis in [48], we reproduce the asymptotic behavior (19) of $\alpha_{0,1}$. In general, $\alpha_{n,1}$ approach $\alpha_{n,2}$ while the associated eigenfunctions $v_{k,1}(\bar{r})$ approach $\sqrt{2}\,v_{k,2}(\bar{r})$ as $R_1 \to 0$ (see also [60]). As a consequence, the matrix A, whose elements were defined in equation (A.21) as a weighted scalar product of these functions, approaches $I/\sqrt{2}$, where I is the identity matrix. In the leading order, one gets thus

$$W_{k,k'} \approx \delta_{k,k'} B_k^{(1)} B_{k'}^{(2)}, \tag{A.45}$$

and the diagonal structure of this matrix allows for the explicit inversion of $I+W$. We get therefore:

$$c_{n,2} \approx \frac{V_n}{1 + B_n^{(1)} B_n^{(2)}} \qquad (\rho \to 0), \tag{A.46}$$

where $B_n^{(1)}$ and $B_n^{(2)}$ are given by equations (A.19) and (A.20). Using the asymptotic behavior of the modified Bessel functions, we get in the leading order in ρ:

$$w'(\rho) \approx -\frac{\rho^{-1}}{\frac{K_1(\alpha)}{I_1(\alpha)} - \gamma - \ln(\alpha\rho/2)}, \tag{A.47}$$

from which

$$V_k \approx \frac{2v_{k,2}(\rho)}{(\alpha_{k,2}^2 + \alpha^2)\left[\frac{K_1(\alpha)}{I_1(\alpha)} - \gamma - \ln(\alpha\rho/2)\right]}. \tag{A.48}$$

In other words, we obtained a fully explicit approximate solution which does not require a numerical inversion of the infinite-dimensional matrix $I+W$.

Appendix B. Auxiliary survival probabilities

For completeness, we provide here the well-known expressions for the survival probabilities for one-dimensional and planar diffusions. When the particle diffuses on the interval $(0, L_2)$ with absorbing endpoint 0 and reflecting endpoint L_2, the survival probability reads:

$$S_{1D}(t|z) = 2\sum_{n=0}^{\infty} \frac{\sin(\pi(n+1/2)z/L_2)}{\pi(n+1/2)} e^{-\pi^2(n+1/2)^2 Dt/L_2^2}. \tag{B.1}$$

In turn, if the particle diffuses in an annulus between an inner absorbing circle of radius R_1 and an outer reflecting circle of radius R_2, the Laplace transform of the PDF is given by equation (A.3), while its inverse Laplace transform via the residue theorem yields:

$$S_{2\mathrm{D}}(t|r) = \sum_{n=0}^{\infty} \frac{\rho \nu'_{n,1}(\rho)}{\alpha^2_{n,1}} \nu_{n,1}(r/R_2) e^{-\alpha^2_{n,1} D t/R_2^2}. \tag{B.2}$$

Appendix C. Splitting probability

In this appendix, we consider diffusion in a semi-infinite reflecting cylindrical tube of radius R_2 with a coaxial semi-infinite absorbing pillar of radius R_1: $\Omega = \{(x,y,z) \in \mathbb{R}^3 \,:\, R_1^2 < x^2 + y^2 < R_2^2,\ z < 0\}$. We sketch the computation of the splitting probability $u(r,z)$, i.e. the probability of hitting the annular region at the level $z = 0$ before hitting the cylindrical part of the pillar at $r = R_1$. The splitting probability satisfies:

$$\Delta u = 0 \quad \text{in } \Omega, \tag{C.1a}$$

$$u(R_1, z) = 0, \tag{C.1b}$$

$$u(r, 0) = 1, \tag{C.1c}$$

$$(\partial_r u)(R_2, z) = 0, \tag{C.1d}$$

$$u(r,z) \to 0 \quad (z \to -\infty). \tag{C.1e}$$

In analogy to the derivation in appendix A, one can search the solution as:

$$u(r,z) = \sum_{n=0}^{\infty} c_n \nu_{n,1}(r/R_2)\, e^{\alpha_{n,1} z/R_2}, \tag{C.2}$$

where the coefficients c_n are found from the boundary condition (C.1c) by multiplication by $\bar{r}\nu_{k,1}(\bar{r})$ and integration over $\bar{r}$ from ρ and 1,

$$c_n = \int_{\rho}^{1} \mathrm{d}\bar{r}\, \bar{r}\, \nu_{n,1}(\bar{r}) = \frac{\rho \nu'_{n,1}(\rho)}{\alpha^2_{n,1}}. \tag{C.3}$$

When $|z|/R_2$ is large enough, the leading contribution is given by the first term with the smallest value $\alpha_{0,1}$:

$$u(r,z) \approx C(r)\, e^{\alpha_{0,1} z/R_2}, \tag{C.4}$$

with

$$C(r) = \frac{\rho \nu'_{0,1}(\rho)}{\alpha^2_{0,1}} \nu_{0,1}(r/R_2). \tag{C.5}$$

ORCID iDs

Denis S Grebenkov https://orcid.org/0000-0002-6273-9164
Alexei T Skvortsov https://orcid.org/0000-0001-8202-7052

References

[1] Redner S 2001 *A Guide to First-Passage Processes* (Cambridge: Cambridge University Press)
[2] Rice S 1985 *Diffusion-Limited Reactions* (Amsterdam: Elsevier)
[3] ben-Avraham D and Havlin S 2010 *Diffusion and Reactions in Fractals and Disordered Systems* (Cambridge: Cambridge University Press)
[4] Metzler R, Oshanin G and Redner S (eds) 2014 *First-Passage Phenomena and Their Applications* (Singapore: World Scientific Press)
[5] Lindenberg K, Metzler R and Oshanin G (eds) 2019 *Chemical Kinetics: Beyond the Textbook* (Hackensack, NJ: World Scientific)
[6] Condamin S, Bénichou O, Tejedor V, Voituriez R and Klafter J 2007 First-passage time in complex scale-invariant media *Nature* **450** 77
[7] Grebenkov D S 2007 NMR survey of reflected Brownian motion *Rev. Mod. Phys.* **79** 1077–137
[8] Bénichou O, Chevalier C, Klafter J, Meyer B and Voituriez R 2010 Geometry-controlled kinetics *Nat. Chem.* **2** 472–7
[9] Bénichou O, Loverdo C, Moreau M and Voituriez R 2011 Intermittent search strategies *Rev. Mod. Phys.* **83** 81–130
[10] Höfling F and Franosch T 2013 Anomalous transport in the crowded world of biological cells *Rep. Prog. Phys.* **76** 046602
[11] Bressloff P C and Newby J M 2013 Stochastic models of intracellular transport *Rev. Mod. Phys.* **85** 135–96
[12] Grebenkov D S and Nguyen B-T 2013 Geometrical structure of Laplacian eigenfunctions *SIAM Rev.* **55** 601–67
[13] Grebenkov D S 2020 Paradigm shift in diffusion-mediated surface phenomena *Phys. Rev. Lett.* **125** 078102
[14] Weiss G H 1986 Overview of theoretical models for reaction rates *J. Stat. Phys.* **42** 3
[15] Bénichou O and Voituriez R 2008 Narrow-escape time problem: time needed for a particle to exit a confining domain through a small window *Phys. Rev. Lett.* **100** 168105
[16] Holcman D and Schuss Z 2014 The narrow escape problem *SIAM Rev.* **56** 213–57
[17] Bénichou O and Voituriez R 2014 From first-passage times of random walks in confinement to geometry-controlled kinetics *Phys. Rep.* **539** 225–84
[18] Holcman D and Schuss Z 2015 *Stochastic Narrow Escape in Molecular and Cellular Biology* (New York: Springer)
[19] Grebenkov D S 2016 Universal formula for the mean first passage time in planar domains *Phys. Rev. Lett.* **117** 260201
[20] Guérin T, Levernier N, Bénichou O and Voituriez R 2016 Mean first-passage times of non-Markovian random walkers in confinement *Nature* **534** 356–9
[21] Mattos T, Mejía-Monasterio C, Metzler R and Oshanin G 2012 First passages in bounded domains: when is the mean first passage time meaningful? *Phys. Rev.* E **86** 031143
[22] Godec A and Metzler R 2016 Universal proximity effect in target search kinetics in the few encounter limit *Phys. Rev.* X **6** 041037
[23] Godec A and Metzler R 2016 First passage time distribution in heterogeneity controlled kinetics: going beyond the mean first passage time *Sci. Rep.* **6** 20349
[24] Grebenkov D S, Metzler R and Oshanin G 2018 Strong defocusing of molecular reaction times results from an interplay of geometry and reaction control *Commun. Chem.* **1** 96
[25] Reva M, DiGregorio D A and Grebenkov D S 2021 A first-passage approach to diffusion-influenced reversible binding: insights into nanoscale signaling at the presynapse *Sci. Rep.* **11** 5377
[26] Hughes B D 1995 *Random Walks and Random Environments* (Oxford: Clarendon)
[27] Levernier N, Dolgushev M, Bénichou O, Voituriez R and Guérin T 2019 Survival probability of stochastic processes beyond persistence exponents *Nat. Commun.* **10** 2990
[28] Kayser R F and Hubbard J B 1983 Diffusion in a medium with a random distribution of static traps *Phys. Rev. Lett.* **51** 79–82
[29] Kayser R F and Hubbard J B 1984 Reaction diffusion in a medium containing a random distribution of nonoverlapping traps *J. Chem. Phys.* **80** 1127–30
[30] Torquato S and Avellaneda M 1991 Diffusion and reaction in heterogeneous media: pore-size distribution, relaxation times and mean survival time *J. Chem. Phys.* **95** 6477–89
[31] Levitz P, Grebenkov D S, Zinsmeister M, Kolwankar K M and Sapoval B 2006 Brownian flights over a fractal nest and first passage statistics on irregular surfaces *Phys. Rev. Lett.* **96** 180601

[32] Lanoiselée Y, Moutal N and Grebenkov D S 2018 Diffusion-limited reactions in dynamic heterogeneous media *Nat. Commun.* **9** 4398
[33] Basnayake K, Hubl A, Schuss Z and Holcman D 2018 Extreme narrow escape: shortest paths for the first particles among n to reach a target window *Phys. Lett.* A **382** 3449–54
[34] Grebenkov D S, Metzler R and Oshanin G 2022 Search efficiency in the Adam–Dëlbruck reduction-of-dimensionality scenario versus direct diffusive search *New J. Phys.* **24** 083035
[35] Varadhan S R S 1967 On the behavior of the fundamental solution of the heat equation with variable coefficients *Commun. Pure Appl. Math.* **20** 431–55
[36] Varadhan S R S 1967 Diffusion processes in a small time interval *Commun. Pure Appl. Math.* **20** 659–85
[37] Smith N R and Meerson B 2019 Geometrical optics of constrained Brownian excursion: from the KPZ scaling to dynamical phase transitions *J. Stat. Mech.* 023205
[38] Meerson B and Oshanin G 2022 Geometrical optics of large deviations of fractional Brownian motion *Phys. Rev.* E **105** 064137
[39] Carslaw H S and Jaeger J C 1959 *Conduction of Heat in Solids* 2nd edn (Oxford: Oxford University Press)
[40] Crank J 1956 *The Mathematics of Diffusion* (Oxford: Oxford University Press)
[41] Thambynayagam R K M 2011 *The Diffusion Handbook: Applied Solutions for Engineers* (New York: McGraw-Hill)
[42] Isaacson S A and Newby J 2013 Uniform asymptotic approximation of diffusion to a small target *Phys. Rev.* E **88** 012820
[43] Rupprecht J-F, Bénichou O, Grebenkov D S and Voituriez R 2015 Exit time distribution in spherically symmetric two-dimensional domains *J. Stat. Phys.* **158** 192–230
[44] Grebenkov D S, Metzler R and Oshanin G 2018 Towards a full quantitative description of single-molecule reaction kinetics in biological cells *Phys. Chem. Chem. Phys.* **20** 16393
[45] Grebenkov D S, Metzler R and Oshanin G 2019 Full distribution of first exit times in the narrow escape problem *New J. Phys.* **21** 122001
[46] Grebenkov D S, Metzler R and Oshanin G 2021 Distribution of first-reaction times with target sites on boundaries of shell-like regions *New J. Phys.* **23** 123049
[47] Grebenkov D S 2020 Diffusion toward non-overlapping partially reactive spherical traps: fresh insights onto classic problems *J. Chem. Phys.* **152** 244108
[48] Grebenkov D S and Skvortsov A T 2022 Diffusion towards a nanoforest of absorbing pillars *J. Chem. Phys.* **157** 244102
[49] Grebenkov D S and Krapf D 2018 Steady-state reaction rate of diffusion-controlled reactions in sheets *J. Chem. Phys.* **149** 064117
[50] Delitsyn A and Grebenkov D S 2018 Mode matching methods in spectral and scattering problems *Q. J. Mech. Appl. Math.* **71** 537–80
[51] Delitsyn A and Grebenkov D S 2022 Resonance scattering in a waveguide with identical thick perforated barriers *Appl. Math. Comput.* **412** 126592
[52] Keller K H and Stein T R 1967 A two-dimensional analysis of porous membrane transport *Math. Biosci.* **1** 421–37
[53] Cai X and Wallis G B 1992 Potential flow around a row of spheres in a circular tube *Phys. Fluids* A **4** 904
[54] Yuste S B, Abad E and Lindenberg K 2013 Exploration and trapping of mortal random walkers *Phys. Rev. Lett.* **110** 220603
[55] Meerson B and Redner S 2015 Mortality, redundancy and diversity in stochastic search *Phys. Rev. Lett.* **114** 198101
[56] Grebenkov D S and Rupprecht J-F 2017 The escape problem for mortal walkers *J. Chem. Phys.* **146** 084106
[57] Meerson B 2019 Mortal Brownian motion: three short stories *Int. J. Mod. Phys.* B **33** 1950172
[58] Talbot A 1979 The accurate numerical inversion of Laplace transforms *IMA J. Appl. Math.* **23** 97–120
[59] Maz'ya V G, Nazarov S A and Plamenevskii B A 1985 Asymptotic expansions of the eigenvalues of boundary value problems for the Laplace operator in domains with small holes *Math. USSR Izv.* **24** 321–45
[60] Ward M J and Keller J B 1993 Strong localized perturbations of eigenvalue problems *SIAM J. Appl. Math.* **53** 770–98

[61] Kolokolnikov T, Titcombe M S and Ward M J 2005 Optimizing the fundamental Neumann eigenvalue for the Laplacian in a domain with small traps *Eur. J. Appl. Math.* **16** 161
[62] Cheviakov A F and Ward M J 2011 Optimizing the principal eigenvalue of the Laplacian in a sphere with interior traps *Math. Comput. Model.* **53** 1394–409
[63] Chaigneau A and Grebenkov D S 2022 First-passage times to anisotropic partially reactive targets *Phys. Rev.* E **105** 054146
[64] Sandua T, Boldeiu G and Moagar-Poladian V 2013 Applications of electrostatic capacitance and charging *J. Appl. Phys.* **114** 224904
[65] Berg H C and Purcell E M 1977 Physics of chemoreception *Biophys. J.* **20** 193
[66] Berezhkovskii A M and Barzykin A V 2007 Simple formulas for the trapping rate by nonspherical absorber and capacitance of nonspherical conductor *J. Chem. Phys.* **126** 106102
[67] Lindsay A E, Bernoff A J and Ward M J 2017 First passage statistics for the capture of a Brownian particle by a structured spherical target with multiple surface traps *Multiscale Model. Simul.* **15** 74–109
[68] Grebenkov D S and Skvortsov A T 2022 Mean first-passage time to a small absorbing target in three-dimensional elongated domains *Phys. Rev.* E **105** 054107
[69] Berezhkovskii A M, Makhnovskii Y A, Monine M I, Zitserman V Y and Shvartsman S Y 2004 Boundary homogenization for trapping by patchy surfaces *J. Chem. Phys.* **121** 11390
[70] Bernoff A J, Lindsay A E and Schmidt D D 2018 Boundary homogenization and capture time distributions of semipermeable membranes with periodic patterns of reactive sites *Multiscale Model. Simul.* **16** 1411–47
[71] Bernoff A J and Lindsay A E 2018 Numerical approximation of diffusive capture rates by planar and spherical surfaces with absorbing pores *SIAM J. Appl. Math.* **78** 266–90
[72] Mörters P and Peres Y 2010 *Brownian Motion* (*Cambridge Series in Statistical and Probabilistic Mathematics*) (New York: Cambridge University Press)
[73] Koplik J, Redner S and Hinch E J 1994 Tracer dispersion in planar multipole flows *Phys. Rev.* E **50** 4650
[74] Koplik J, Redner S and Hinch E J 1995 Universal and nonuniversal first-passage properties of planar multipole flows *Phys. Rev. Lett.* **74** 82
[75] Levitz P E, Zinsmeister M, Davidson P, Constantin D and Poncelet O 2008 Intermittent Brownian dynamics over a rigid strand: Heavily tailed relocation statistics *Phys. Rev.* E **78** 030102(R)
[76] Grebenkov D S 2021 Statistics of boundary encounters by a particle diffusing outside a compact planar domain *J. Phys. A.: Math. Theor.* **54** 015003
[77] Kharisov B I, Kharissova O V, García B O, Méndez Y P and de la Fuente I G 2015 State of the art of nanoforest structures and their applications *RSC Adv.* **5** 105507
[78] Davis A M J and Lauga E 2010 Hydrodynamic friction of fakir–like superhydrophobic surfaces *J. Fluid Mech.* **661** 402–11
[79] Ramon G Z, Wong M C Y and Hoek E M V 2012 Transport through composite membrane, part 1: is there an optimal support membrane? *J. Membr. Sci.* **415–416** 298–305
[80] Ramon G Z and Hoek E M V 2013 Transport through composite membranes, part 2: impacts of roughness on permeability and fouling *J. Membr. Sci.* **425–426** 141–8
[81] Nair P R and Alam M A 2007 Dimensionally frustrated diffusion towards fractal adsorber *Phys. Rev. Lett.* **99** 256101
[82] Chen G, Guan R, Shi M, Dai X, Li H, Zhou N, Chen D and Mao H 2022 A nanoforest-based humidity sensor for respiration monitoring *Microsyst. Nanoeng.* **8** 44
[83] Borberg E *et al* 2019 Light-controlled selective collection-and-release of biomolecules by an on-chip nanostructured device *Nano Lett.* **19** 5868–78
[84] Watson G N 1962 *A Treatise on the Theory of Bessel Functions* (Cambridge: Cambridge University Press)